



Contents lists available at ScienceDirect

Bioorganic & Medicinal Chemistry Letters

journal homepage: www.elsevier.com/locate/bmcl

Structure-based design of substituted hexafluoroisopropanol-aryl-sulfonamides as modulators of RORc

Benjamin P. Fauber^{a,*}, Gladys de Leon Boenig^a, Brenda Burton^b, Céline Eidenschenk^a, Christine Everett^a, Alberto Gobbi^a, Sarah G. Hymowitz^a, Adam R. Johnson^a, Marya Liimatta^a, Peter Lockey^b, Maxine Norman^b, Wenjun Ouyang^a, Olivier René^a, Harvey Wong^a

^aGenentech, Inc., 1 DNA Way, South San Francisco, CA 94080, USA

^bArgenta, Units 7–9 Spire Green Centre, Flex Meadow, Harlow, Essex CM19 5TR, UK

ARTICLE INFO

Article history:

Received 20 September 2013

Revised 23 October 2013

Accepted 25 October 2013

Available online 4 November 2013

Keywords:

RORc

RORγ

T0901317

X-ray structure

IL-17

Inflammation

Autoimmune

ABSTRACT

The structure–activity relationships of T0901317 analogs were explored as RORc inverse agonists using the principles of property- and structure-based drug design. An X-ray co-crystal structure of T0901317 and RORc was obtained and provided molecular insight into why T0901317 functioned as an inverse agonist of RORc; whereas, the same ligand functioned as an agonist of FXR, LXR, and PXR. The structural data was also used to design inhibitors with improved RORc biochemical and cellular activities. The improved inhibitors possessed enhanced selectivity profiles (rationalized using the X-ray crystallographic data) against other nuclear receptors.

© 2013 Elsevier Ltd. All rights reserved.

T_H-17 cells are a subset of pro-inflammatory CD4⁺ T cells whose production of IL-17 is dependent upon the nuclear receptor (NR) retinoic acid receptor-related orphan receptor gamma (RORγ or RORc, also known as NR1F3).¹ IL-17 has been implicated in the pathology of several autoimmune diseases including rheumatoid arthritis (RA), inflammatory bowel disease, psoriasis, and multiple sclerosis.² Reduced IL-17 expression via antibody blockade or genetic knock-out in mice resulted in a marked decrease in inflammation in several murine models.^{3,4} Monoclonal neutralizing antibodies against IL-17 are also being evaluated in human clinical trials and have demonstrated proof-of-concept activity in psoriasis, RA, and non-infectious uveitis.⁵

In addition to modulating the expression of the IL-17 family of cytokines, RORc signaling promotes other pro-inflammatory cytokines including IL-22 and GM-CSF in T_H17 cells.^{6,7} Thus, inhibition of RORc may lead to enhanced anti-inflammatory activity over the IL-17-neutralizing antibodies that are currently under investigation in clinical trials. These observations, coupled with the viability of RORc genetic knock-out mice,^{8,9} make RORc an attractive target for modulating human autoimmune diseases.^{10,11}

* Corresponding author. Tel.: +1 650 467 5773.

E-mail address: Fauber.Benjamin@gene.com (B.P. Fauber).

The benzene-sulfonamide compound T0901317 (Fig. 1, compound **1**) was initially described by a team at Tularik (now Amgen) as a potent agonist of the liver X receptor (LXR).¹² Since the original disclosure of **1**, other investigators have demonstrated that **1** is an agonist of multiple additional NRs including pregnane X receptor (PXR) and farnesoid X receptor (FXR).^{13,14} Recently, a team from the Scripps Research Institute in Florida described **1** as an inverse agonist of RORc.¹⁵ We were intrigued by the binding of **1** to RORc, and embarked upon a campaign to explore the SAR of related analogs as inverse agonists of RORc.

In an effort to aid our analog design, we co-crystallized compound **1** with the human RORc ligand-binding domain (LBD) and obtained a 2.9 Å resolution X-ray structure (Table S1 Supplementary data).¹⁶ The helices of the RORc LBD co-crystal structure adopted the canonical three-layered α-helical fold common to most NRs,¹⁷ with **1** buried in the hydrophobic core (Fig. S1a, Supplementary Data). The RORc LBD helices were in a similar arrangement to that of the previously reported co-crystal structure of the RORc LBD with 25-hydroxycholesterol (Fig. 1, compound **2**) [PDB: 3L0L],¹⁸ with the exception that there is a lack of density for the C-terminus of helix 11, all of helix 11' and helix 12 in the co-crystal structure with **1**, suggesting these helices lack regular structure when RORc interacts with compound **1**. The disordered helix 12 should disfavor recruitment of co-activator proteins by prohibiting

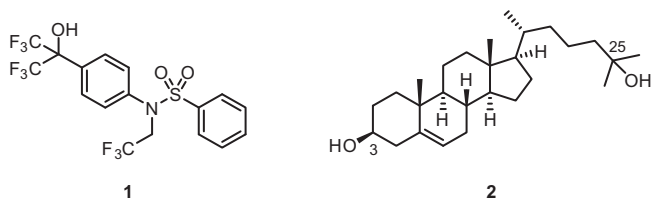


Figure 1. Chemical structures of T0901317 (**1**) and 25-hydroxycholesterol (**2**).

the interaction of Glu483 on helix 12 with the conserved LXXLL ‘charge-clamp’ motif in co-activator proteins.¹⁹ This structural observation was concordant with the RORc LBD and steroid receptor co-activator-1 (SRC1) recruitment biochemical assay results in which **2** behaved as an agonist; whereas, **1** was an inverse agonist.^{15,18}

Within the ligand binding pocket of the RORc co-crystal structure, the hexafluoro-2-isopropanol moiety of **1** could fit in two equal but opposite orientations of the $2F_o - F_c$ electron density map (Fig. S1b, Supplementary data). In both orientations of the hexafluoroisopropanol moiety, there were no notable hydrogen bonds (<3.2 Å) from the hydroxyl group to the protein or crystallographic water molecules. This observation was in stark contrast to the co-crystal structures of **1** with the LBDs of human LXR α [PDB: 1UHL]²¹ and LXR β [PDB: 1UPV],²² where the hexafluoroisopropanol hydroxyl group made a strong hydrogen bond interaction with a histidine residue in LXR α (His421, 2.4 Å) and LXR β (His435, 2.5 Å), resulting in stabilization of helices 11–12, recruitment of the co-activator, and receptor agonist activity.²³ The lack of a hydrogen bond interaction between **1** and His458 in RORc may explain why this ligand behaved as an inverse agonist of RORc.

In addition to the lack of ligand hydrogen bonding in the RORc co-crystal structure, **1** was also rotated $\sim 30^\circ$ in the binding pocket relative to its orientation in the LXR co-structures (Fig. 2a). The residue difference that potentially enforced the $\sim 30^\circ$ rotation of **1** was the presence of Leu303 in RORc, which was a smaller alanine residue in LXR α (Ala261) and LXR β (Ala275). The planar rotation of

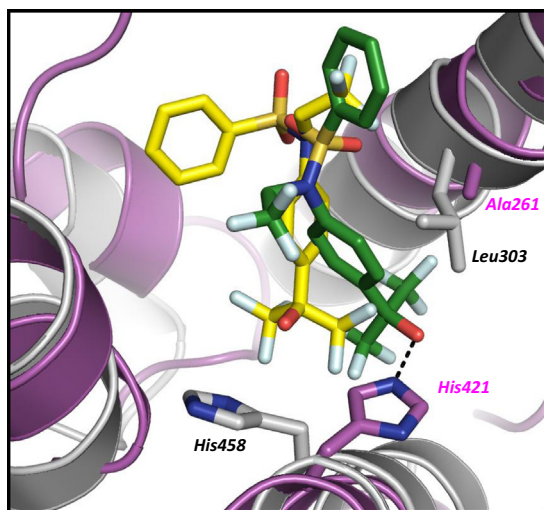


Figure 2a. A 2.9 Å resolution co-crystal structure of compound **1** (yellow) in complex with RORc (grey) and a 2.9 Å resolution co-crystal structure of compound **1** (green) in complex with LXR α (magenta) [PDB: 1UHL]. All atoms of the LBD for each receptor have been overlaid. His435 (grey) in RORc does not make a notable hydrogen bond interactions (<3.2 Å) with **1** (yellow); whereas, **1** (green) does make a strong hydrogen bond (2.4 Å) with His421 (magenta) in LXR α . Hydrogen bonds are shown as dashed lines (black). The Leu303 (grey) side-chain in RORc is a smaller Ala261 (magenta) in LXR α and the residue difference potentially gives rise to different rotations of the ligand in the respective receptors.

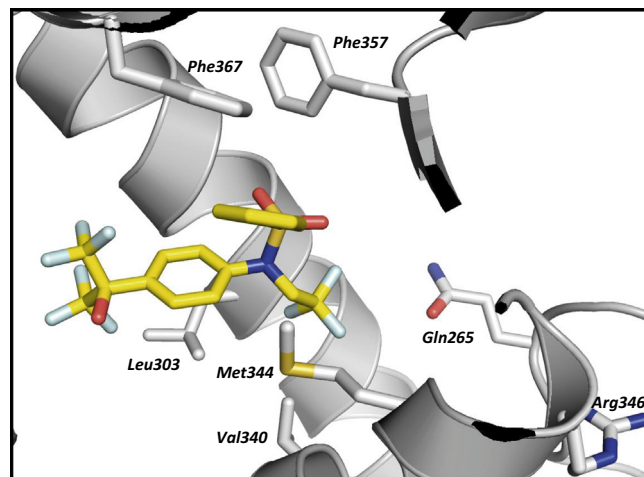


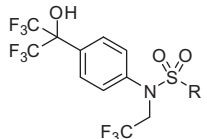
Figure 2b. Co-crystal structure of compound **1** (yellow) in complex with RORc (grey). The phenyl-sulfonamide group of compound **1** accessed a parallel-displaced π - π stacking interaction with Phe367 (3.3–3.6 Å), and Phe367 engaged neighboring Phe357 in an edge-to-face π - π stacking interaction (3.9–4.0 Å). Leu303 (grey), Val340 (grey), and Met344 (grey) made notable hydrophobic contacts with compound **1**. The ligand binding pocket polar residues Gln265 (grey) and Arg346 (grey) are also depicted.

the ligand, along with other residue differences in the receptors, gave rise to a unique binding orientation of **1** in RORc relative to that observed in co-structures of **1** with LXR α , LXR β , and PXR [PDB: 209I].²⁴ As a result of the unique binding orientation of **1** in RORc, the phenyl-sulfonamide group of **1** was allowed to access a parallel-displaced π - π stacking interaction with Phe367 (3.3–3.6 Å).²⁵ The π - π stacking interaction of **1** and Phe367 was further enhanced by the edge-to-face π - π stacking interaction of Phe367 with neighboring Phe357 (3.9–4.0 Å) (Fig. 2b). The aforementioned receptor–ligand π - π stacking interaction was not observed in the LXR and PXR co-structures with **1**. We predicted that compounds capable of forming receptor–ligand π - π stacking interactions with Phe367 in RORc could exhibit increased RORc potency and selectivity.²⁶ In order to test this hypothesis, we designed and synthesized aryl-sulfonamide analogs of **1**, allowing exploration of their structure–activity relationships.

We evaluated analogs of **1** in two biochemical assays.²⁷ A radioligand competition binding assay provided information on the binding affinity of a compound for the RORc LBD by displacement of a tritiated 25-hydroxycholesterol radioligand from the RORc ligand binding pocket. A co-activator peptide binding assay monitored the ability of the RORc LBD to bind to a co-activator peptide derived from SRC1. Disrupting the recruitment of the SRC1 co-activator peptide is indicative of compounds that display inverse agonist activity with RORc.

In addition to optimizing the complementarity of the ligand to the RORc binding pocket, we paid close attention to the calculated log P value (clog P <5 was preferred) of potential analogs, as our starting molecule (**1**) was fairly lipophilic (clog P = 4.5).²⁸ Our goal was to explore the SAR of T0901317 analogs against RORc while maintaining favorable physicochemical properties to favor drug-like pharmaceutical properties.^{29,30} Thus, we initiated our exploration of the phenyl-sulfonamide moiety via a Hansch analysis with a nitrile substituent (Table 1, compounds **3–5**, clog P = 4.4–4.2, respectively).³¹ It was clear from the Hansch analysis that the *para*-nitrile substituent (**5**) was preferred and provided a slight improvement in the ligand-lipophilicity efficiency (LLE)³² value versus **1**, while it maintained similar potency values in the RORc binding and SRC1 recruitment assays. In an effort to probe the effects of various *para*-substituents, we synthesized and tested a set of analogs with

Table 1
Structure–activity relationships of the sulfonamide analogs



Compd	R-group	RORc IC ₅₀ ^a (μM)	RORc LLE ^b	RORc SRC1 EC ₅₀ ^c (μM) [%eff.]
1	Ph	0.060	2.7	0.054 [−99%]
3	(2-CN)Ph	0.520	1.9	0.920 [−91%]
4	(3-CN)Ph	0.190	2.4	0.100 [−93%]
5	(4-CN)Ph	0.050	3.1	0.061 [−96%]
6	(4-Me)Ph	0.051	2.3	0.020 [−100%]
7	(4-F)Ph	0.034	2.8	0.019 [−99%]
8	3-Pyridyl	0.748	2.7	1 [−88%]
9	5-(2-N-Me)pyrazole	4	2.1	ND
10	c-Pr	5	1.9	ND
11	Bn	0.520	2.1	>2 [−22%]

See the [Supplementary data](#) for experimental details associated with each assessment. All assay results are reported as the arithmetic mean of at least two separate runs. ND = not determined.

^a Inhibition of the RORc LBD and [³H₂]-25-hydroxycholesterol interaction.

^b Ligand-lipophilicity efficiency (LLE) was calculated using the RORc biochemical IC₅₀ value and calculated log *P*.³²

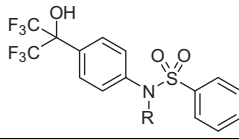
^c Inhibition of RORc LBD recruitment of the SRC1 co-activator peptide; negative percent efficacy denotes inverse agonism relative to the basal activity of apo-RORc LBD.

different σ_p values (Table 1, compounds **6** and **7**).^{33,34} The (*para*-fluorophenyl)-sulfonamide moiety (**7**) provided an appropriate balance between RORc binding potency, LLE, and potent full inverse agonism in the SRC1 peptide binding assay. Exploration of aromatic heterocyclic-sulfonamide analogs did not provide any potency improvements (Table 1, compounds **8** and **9**). The lack of potency from the cyclopropyl-sulfonamide analog demonstrated that the partial *sp*² character present in the cyclopropane ring was not sufficient to engage the aforementioned π - π stacking interaction with the Phe367 residue in the RORc ligand binding site (Table 1, compound **10**).³⁵ Extending the aromatic moiety by one atom to generate a benzylic-sulfonamide analog resulted in a loss of binding affinity, presumably due to a disruption of the π - π stacking interaction with the receptor (Table 1, compound **11**).

As discussed above, the phenyl-sulfonamide group on **1** accessed a unique π - π stacking interaction in the RORc co-crystal structure that was not observed in the co-structures of **1** with LXR and PXR. As a result of the phenyl-sulfonamide moiety adopting a unique orientation, the *N*-2,2,2-trifluoroethyl group also accessed a different vector than those previously observed in LXR or PXR. The *N*-trifluoroethyl group resided in a region of the RORc ligand binding pocket rich in lipophilic residues, and it made several lipophilic interactions³⁶ (3.3–3.4 Å) with Leu303, Val340, and Met344 (Fig. 2b). We were intrigued that in the same region of the RORc ligand binding pocket, the 3 β -OH of 25-hydroxycholesterol (**2**) formed a direct hydrogen bond with Gln265 (3.1 Å) and interacted with Arg346 via a water-mediated hydrogen bond (2.8 Å) [PDB: 3LOL]. Thus, we initiated an exploration of various *N*-alkyl analogs of **1** to probe the potential engagement of the Gln265 or Arg346 residues in the RORc ligand binding pocket.

Exploration of *N*-alkyl analogs of **1** commenced with the synthesis of an ethyl-alcohol analog (Table 2, compound **12**). The hydroxyl group on **12** was poorly tolerated and resulted in a significant loss in potency. Computational modeling studies with this analog suggest that the lipophilic region surrounding the *N*-trifluoroethyl group in the co-crystal structure of **1** and RORc may not tolerate polar functionality. We hypothesized that if the ethyl-alcohol

Table 2
Structure–activity relationships of the *N*-alkyl analogs



Compd	R-group	RORc IC ₅₀ ^a (μM)	RORc LLE ^b	RORc SRC1 EC ₅₀ ^c (μM) [%eff.]
12	(CH ₂) ₂ OH	4	2.3	1 [−80%]
13	(CH ₂) ₂ OMe	3	1.8	>10
14	(CH ₂) ₂ SO ₂ Me	>10	—	>10
15	(CH ₂) ₂ NHCOMe	>10	—	>10
16	(CH ₂) ₂ CO ₂ H	>10	—	>10
17	Et	0.245	2.3	0.190 [−97%]
18	(CH ₂) ₂ CF ₃	0.519	1.4	4 [−70%]
19	Bn	0.467	1.0	8 [−64%]
20	H	>10	—	ND

See the [Supplementary data](#) for experimental details associated with each assessment. All assay results are reported as the arithmetic mean of at least two separate runs. ND = not determined.

^a Inhibition of the RORc LBD and [³H₂]-25-hydroxycholesterol interaction.

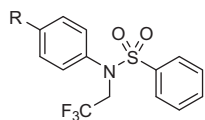
^b Ligand-lipophilicity efficiency (LLE) was calculated using the RORc biochemical IC₅₀ value and calculated log *P*.³²

^c Inhibition of RORc LBD recruitment of the SRC1 co-activator peptide; negative percent efficacy denotes inverse agonism relative to the basal activity of apo-RORc LBD.

could not directly interact with the Gln265, it may be able to indirectly interact with the Gln265 or Arg346 via a water-mediated hydrogen bond network. We made additional attempts to directly engage those RORc binding pocket polar residues, or indirectly interact with them via water-mediated hydrogen bonding. Several analogs containing a range of *N*-alkyl polar side chains were synthesized, and these analogs were also poorly tolerated in the RORc biochemical assays (Table 2, compounds **13**–**16**). After exploring polar substitution, we focused our attention on lipophilic *N*-alkyl substituents. The *N*-ethyl analog was synthesized to explore the influence of the 2,2,2-trifluoroethyl substituent on potency and also potentially improve the LLE value (Table 2, compound **17**). As it turned out, the potency values of compound **17** in the binding assay and the SRC1 recruitment assay were approximately fourfold less than the parent molecule (**1**) and **17** provided no improvement in LLE. The *N*-3,3,3-trifluoropropyl and *N*-benzyl analogs were synthesized to explore the role of larger lipophilic groups in the RORc binding pocket (Table 2, compounds **18** and **19**). Both analogs had similar RORc biochemical potency, but they were inferior to the potency of **1**. Additionally, replacement of the *N*-alkyl group with a hydrogen resulted in an inactive molecule (Table 2, compound **20**), and thus confirmed the importance of the *N*-2,2,2-trifluoroethyl group in maintaining RORc binding affinity.

The hexafluoro-2-isopropanol moiety of **1** binds near the interface of helix 11 and helix 3 in the RORc co-crystal structure. As mentioned above, the alcohol on the hexafluoroisopropanol group did not make any notable hydrogen bonds to the adjacent protein residues or to the crystallographic water molecules. To investigate the importance of the alcohol functionality, we synthesized the hexafluoroisopropanol *O*-methyl ether. It lost considerable binding and functional potency in the RORc biochemical assays (Table 3, compound **21**). Computational docking studies initially suggested that there could be space to accommodate the hexafluoroisopropanol *O*-methyl ether, given the distribution of the 2*F*_o–*F*_c electron density map in the hexafluoroisopropanol containing region of the ligand (**1**) co-crystal structure with RORc. The decrease in RORc biochemical activity for compound **21** also suggested that there may have been an interaction with the alcohol that was not apparent in the 2.9 Å resolution co-crystal structure of **1** and RORc. To

Table 3
Structure–activity relationships of the hexafluoro-2-isopropanol group



Compd	R-group	RORc IC ₅₀ ^a (μM)	RORc LLE ^b	RORc SRC1 EC ₅₀ ^c (μM) [%eff.]
21	C(CF ₃) ₂ OMe	0.900	0.6	9 [–45%]
22	CH ₂ OH	>10	–	>10
23	CO ₂ H	>10	–	>10
24	CONH ₂	>10	–	>10
25	SO ₂ NH ₂	9	2.7	>10

See the [Supplementary data](#) for experimental details associated with each assessment. All assay results are reported as the arithmetic mean of at least two separate runs.

^a Inhibition of the RORc LBD and [³H₂]-25-hydroxycholesterol interaction.

^b Ligand-lipophilicity efficiency (LLE) was calculated using the RORc biochemical IC₅₀ value and calculated logP.³²

^c Inhibition of RORc LBD recruitment of the SRC1 co-activator peptide; negative percent efficacy denotes inverse agonism relative to the basal activity of apo-RORc LBD.

probe the importance of various ligand hydrogen bond donors in that region of the ligand binding pocket, we synthesized analogs containing a benzylic alcohol, a carboxylic acid, a primary amide, and a primary sulfonamide (Table 3, compounds **22–25**, respectively). All of these analogs had negligible activity in both RORc biochemical assays. These results suggested that the loss of potency observed with compound **21** was probably due to a steric requirement of the RORc binding pocket that did not favor the O-methyl ether moiety.

In an attempt to explore alternative binding modes of the ligand, we explored several core change analogs of **1** (Table 4). Two isomers of the *N*-ethyl analog were examined as comparisons to the parent *N*-ethyl sulfonamide compound **17**. Cyclization of the *N*-ethyl group onto the core phenyl ring to generate an indoline *N*-benzene-sulfonamide analog was less potent than the parent compound (Table 4, compound **26**). Movement of the *N*-ethyl-*N*-phenylsulfonamide group to the *meta*-position of the core phenyl ring also resulted in loss of potency in the RORc binding assay and a several-fold loss of potency in the SRC1 co-activator recruitment assay (Table 4, compound **27**). In a comparison of functional groups, the sulfonamide moiety of **1** was converted into an amide, resulting in a large potency decrease (Table 4, compound **28**). This large drop in potency was somewhat anticipated given the major differences in the conformational preferences of sulfonamides and amides.³⁷ Removal of the *N*-2,2,2-trifluoroethyl group on **28** resulted in a further loss of potency (Table 4, compound **29**), similar to that observed in the previous comparison of compounds **1** and **20**.

During the course of our SAR studies, we synthesized several of the published ROR modulators as control compounds—including SR1078.³⁸ We found that SR1078 lacked detectable binding potency in our radiometric assay and lacked activity in our SRC1 co-activator recruitment assay (Table 4, compound **30**). A similar observation was recently described by a team at GlaxoSmithKline using an analogous co-activator recruitment assay.²⁰ The related sulfonamide analog, SR1001,³⁹ also displayed limited potency in our RORc biochemical assays (Table 4, compound **31**).

We also profiled the potent inverse agonist compounds identified with the SRC1 co-activator recruitment assay in a series of HEK293-Gal4 construct ROR cellular assays. Three known isoforms of ROR (RORc, RORb, and RORa) were profiled under cellular receptor antagonist conditions by which we monitored the suppression of their basal transcriptional activity. In order to assess the NR

cellular selectivity of the potent inverse agonists, these compounds were also subjected to a panel of LXR, PXR, and FXR HEK293-Gal4 construct cell assays and we monitored the activation/agonism of their basal transcriptional activity to determine if there were any improvements in selectivity versus compound **1**. Ultimately, the most potent and selective compounds identified in the ROR and NR cell assay panels were progressed into a cytokine assay that monitored their ability to inhibit IL-17 production in an isolated human peripheral blood mononuclear cell (PBMC) fraction. We also used interferon gamma (INFγ) and CellTiter-Glo® (CTG) cell culture assays as positive controls to monitor for activity against non-T_H17 cell cytokines and aberrant cytotoxicity, respectively.²⁷

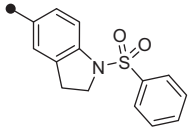
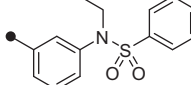
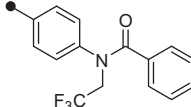
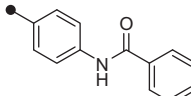
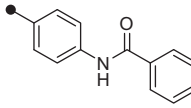
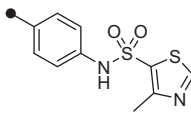
A key weakness in using **1** to assess the effect of RORc inhibition in cellular or in vivo studies is its lack of selectivity for RORc over other NRs. In particular, while compound **1** was a 463 nM inhibitor in the RORc Gal4 cellular assay, it was only approximately tenfold selective against the other ROR family members (Table 5). Further, compound **1** was a weak FXR agonist (EC₅₀ = 1 μM) but was a potent LXRα and LXRβ agonist, with 373 and 156 nM EC₅₀ values, respectively, and 643- and 284-fold activation of these receptors, respectively.

Several of our compounds showed improvements in these respects as they possess increased potency and selectivity relative to compound **1**. For instance, compound **5** demonstrated increased inverse agonism of RORc (EC₅₀ = 192 nM) and better selectivity over the other ROR family members. Compound **5** also elicited a weaker agonist response in FXR, LXRβ, and PXR, with no detectable LXRα agonist activity (Table 5). Compound **17** was a modest inhibitor of the SRC1 co-activator assay and this potency, in turn, translated into modest inhibition of the RORc Gal4 cellular assay (EC₅₀ = 593 nM). Compound **17** also displayed limited agonist activity in the FXR and LXRα cell assays, and comparable levels of LXRβ and PXR agonist activity to that noted with compound **1**. Compound **7** displayed potent inhibition in the RORc Gal4 cellular assay (EC₅₀ = 89 nM) and was also >60-fold selective over the other ROR family members. Compound **7** also provided less potent and lower-fold agonist activity in the FXR and LXR cellular assays than that observed with compound **1**. Compound **7** retained the same-fold activation of the PXR receptor as seen with compound **1**, but was fivefold less potent.

The improved selectivity profiles noted with compounds **5** and **7** were potentially due to the successful application of structure-based design principals. Both of these compounds were designed to have an improved receptor–ligand π–π stacking interaction with the RORc Phe367 ligand binding pocket residue. As noted earlier, this π–π stacking interaction was not observed in co-structures of **1** with LXR and PXR. Thus, providing this interaction between compounds and RORc was not expected to facilitate interactions with LXR and PXR and, in turn, increased the selectivity window for RORc.

Compounds **1**, **5**, and **7** were progressed into human primary cell cytokine production assays to assess their abilities to inhibit production of the pro-inflammatory cytokine, IL-17.⁴⁰ Compound **1** displayed modest inhibition of IL-17 (EC₅₀ = 3 μM), while compound **5** was threefold more potent (EC₅₀ = 1 μM). The differences in IL-17 inhibition values between the two compounds exhibited roughly the same difference in potency observed in the RORc Gal4 cellular assay for the two compounds, providing confidence that our early-stage assays were accurately rank-ordering compounds. It was also noteworthy that neither compound showed any activity in the INFγ or CTG assays, demonstrating that the compounds were not indiscriminately suppressing cytokine production, nor were they grossly cytotoxic. Compound **7** was the most potent inhibitor of IL-17 expression (EC₅₀ = 132 nM), with no detectable inhibition in the INFγ and CTG assays (Table 6).

Table 4
Structure–activity relationships of the core change analogs

Compd	R-group			
		RORc IC ₅₀ ^a (μM)	RORc LLE ^b	RORc SRC1 EC ₅₀ ^c (μM) [%eff.]
26		0.883	2.2	5 [–76%]
27		0.329	2.2	0.900 [–94%]
28		2	2.1	4 [–79%]
29		>10	–	>10
30		>10	–	>10
31		2	4.0	0.911 [–88%]

See the [Supplementary data](#) for experimental details associated with each assessment. All assay results are reported as the arithmetic mean of at least two separate runs.

^a Inhibition of the RORc LBD and [³H₂]-25-hydroxycholesterol interaction.

^b Ligand–lipophilicity efficiency (LLE) was calculated using the RORc biochemical IC₅₀ value and calculated log*P*.³²

^c Inhibition of RORc LBD recruitment of the SRC1 co-activator peptide; negative percent efficacy denotes inverse agonism relative to the basal activity of apo-RORc LBD.

Table 5
Potency and selectivity profiles in Gal4 human NR transcription reporter assays^a

Compd	RORc EC ₅₀ (μM)	RORb EC ₅₀ (μM)	RORa EC ₅₀ (μM)	FXR EC ₅₀ ^b (μM) [act.]	LXRα EC ₅₀ ^b (μM) [act.]	LXRβ EC ₅₀ ^b (μM) [act.]	PXR EC ₅₀ ^b (μM) [act.]
1	0.463	6	5	1 [77]	0.373 [643]	0.156 [284]	0.036 [22]
5	0.192	5	7	3 [46]	>10	0.902 [199]	0.571 [27]
7	0.089	6	6	1 [64]	0.719 [303]	0.385 [237]	0.194 [30]
17	0.593	4	5	9 [22]	3 [349]	0.246 [74]	0.039 [24]

See the [Supplementary data](#) for experimental details associated with each assessment. All assay results are reported as the arithmetic mean of at least two separate runs.

^a All assays were conducted in HEK293-Gal4 cellular constructs. All ROR assays monitored the suppression of their respective basal transcriptional activities, an outcome consistent with inverse agonist activity of ligands with these the receptor. The FXR, LXR, and PXR cellular assays monitored the activation of the basal transcriptional activities, an outcome consistent with agonist activity of the receptor.

^b The maximum-fold activation [act.] was the fold increase of the compound's agonist activity relative to the apo-receptor.

Syntheses of the analogs discussed above are described in Scheme S1 ([Supplementary data](#)). The route toward the aryl-sulfonamide analogs commenced with sulfonylation of the commercially available 4-substituted aniline scaffolds under the conditions described by Li et al. (Scheme S1, intermediates **33a–k** and compounds **20** and **31**).⁴¹ The secondary aniline was then alkylated with either an alkyl-halide or alkyl-triflate, in the presence of potassium carbonate and refluxing acetonitrile, to produce various *N*-alkyl analogs (Scheme S1, compounds **1**, **3–13**, **17**, **19**).⁴² The *N*-ethyl(methylsulfone) analog **14** required a modified approach in which compound **20** was treated with 2-chloroethylmethylsulfide and potassium carbonate in warm DMF, followed by oxidation with *m*-CPBA in DCM. Compound **1** was further

transformed into the *O*-methyl ether analog under basic alkylation conditions (Scheme S1, compound **21**). The 4-carboxamide and 4-carboxylic acid core analogs were synthesized from the corresponding nitrile and ester intermediates, respectively (Scheme S1, intermediates **34** and **35**). Hydrolysis of the nitrile intermediate, under basic peroxide conditions,⁴³ produced the primary amide analog, and saponification of the ester intermediate revealed the carboxylic acid analog (Scheme S1, compounds **23** and **24**, respectively).

We also generated analogs using an alternative synthetic sequence in which the aniline nitrogen was first alkylated under basic conditions or reductive amination conditions.⁴⁴ Subsequent sulfonylation or acylation of the secondary aniline intermediates

Table 6
Potency in human IL-17 and INF γ production assays^a

Compd	IL-17 PBMC EC ₅₀ (μ M)	IL-17 PBMC %max. inhibition	INF γ EC ₅₀ (μ M)	CTG EC ₅₀ (μ M)
1	3	81	>20	>20
5	1	74	>20	>20
7	0.132	83	>20	>20

See the [Supplementary data](#) for experimental details associated with each assessment. All assay results are reported as the arithmetic mean of at least two separate runs.

^a All assays were conducted using peripheral blood mononuclear cells (PBMCs) isolated from human whole blood. Interferon gamma (INF γ) and CellTiter-Glo[®] (CTG) cell culture assays were used as positive controls to monitor for non-T_H17 cell cytokine activity and adverse off-target effects on cell physiology, respectively.

provided the final compounds ([Scheme S1](#), compounds **15**, **18**, **25**, and **28**). Compound **16** was made using a similar reaction sequence in which the *N*-alkyl ester group was carried through the synthesis and saponified in the final step to reveal the carboxylic acid group. Compounds **29** and **30** were made via the direct acylation of 2-(4-aminophenyl)-1,1,1,3,3,3-hexafluoropropan-2-ol (**32a**). Compound **27** was generated from intermediate **41** under basic alkylation conditions ([Scheme S2](#), [Supplementary data](#)).⁴¹ Compound **22**²⁴ and compound **26**⁴¹ were synthesized according to literature procedures.

In summary, the structure activity relationships of T0901317 (**1**) analogs were successfully explored to generate improved ROR α inverse agonists using structure-based drug design principles. An X-ray co-crystal structure of **1** and the ROR α LBD facilitated the structure-based drug design efforts. The resulting compounds have improved ROR α biochemical activity, cellular activity, and inhibit IL-17 production in primary human cells. These inhibitors also possess enhanced selectivity profiles against other NRs that can be rationalized using X-ray crystallographic data. This coordinated effort led to the generation of ROR α inverse agonists with suitable biochemical and cellular properties, and will allow investigation of the role of ROR α in autoimmune diseases and other biological roles.

Acknowledgments

We thank Drs. Krista Bowman and Jiansheng Wu and their respective Genentech research groups for performing all required protein expression and purification activities. We also thank Dr. Rene Devos for NR vector expression and Dr. David Chantry for many helpful discussions regarding ROR α . In addition, we thank Crystallographic Consulting, LLC for diffraction data collection. Use of the Advanced Photon Source was supported by the US Department of Energy, Office of Science, Office of Basic Energy Sciences, under Contract No. DE-AC02-06CH11357.

Supplementary data

Supplementary data associated with this article can be found, in the online version, at <http://dx.doi.org/10.1016/j.bmcl.2013.10.054>.

References and notes

- Ivanov, I. I.; McKenzie, B. S.; Zhou, L.; Tadokoro, C. E.; Lepelley, A.; Lafaille, J. J.; Cua, D. J.; Littman, D. R. *Cell* **2006**, *126*, 1121.
- Ouyang, W.; Kolls, J. K.; Zheng, Y. *Immunity* **2008**, *28*, 454.
- Lubberts, E.; Koenders, M. I.; Oppers-Walgreen, B.; van den Bersselaar, L.; Coenen-de Roo, C. J.; Joosten, L. A. *Arthritis Rheum.* **2004**, *50*, 650.
- Nakae, S.; Nambu, A.; Sudo, K.; Iwakura, Y. *J. Immunol.* **2003**, *171*, 6173.
- Patel, D. D.; Lee, D. M.; Kolbinger, F.; Antoni, C. *Ann. Rheum. Dis.* **2013**, *72*, 116.
- Rutz, S.; Eidenschien, C.; Ouyang, W. *Immunol. Rev.* **2013**, *252*, 116.
- Codarri, L.; Gyölvérsi, G.; Tosevski, V.; Hesske, L.; Fontana, A.; Magnenat, L.; Suter, T.; Becher, B. *Nat. Immunol.* **2011**, *12*, 560.
- Kurebayashi, S.; Ueda, E.; Sakaue, M.; Patel, D. D.; Medvedev, A.; Zhang, F.; Jetten, A. M. *Proc. Natl. Acad. Sci. U.S.A.* **2000**, *97*, 10132.
- Sun, Z.; Unutmaz, D.; Zou, Y.-R.; Sunshine, M. J.; Pierani, A.; Brenner-Morton, S.; Mebius, R. E.; Littman, D. R. *Science* **2000**, *288*, 2369.
- Huh, J. R.; Littman, D. R. *Eur. J. Immunol.* **2012**, *42*, 2232.
- Burris, T. P.; Busby, S. A.; Griffin, P. R. *Chem. Biol.* **2012**, *19*, 51.
- Schultz, J. R.; Tu, H.; Luk, A.; Repa, J. J.; Medina, J. C.; Li, L.; Schwendner, S.; Wang, S.; Thoolen, M.; Mangelsdorf, D. J.; Lustig, K. D.; Shan, B. *Genes Dev.* **2000**, *14*, 2831.
- Mitro, N.; Vargas, L.; Romeo, R.; Koder, A.; Saez, E. *FEBS Lett.* **2007**, *581*, 1721.
- Houck, K. A.; Borchert, K. M.; Hepler, C. D.; Thomas, J. S.; Bramlett, K. S.; Michael, L. F.; Burris, T. P. *Mol. Gen. Metab.* **2004**, *83*, 184.
- Kumar, N.; Solt, L. A.; Conkright, J. J.; Wang, Y.; Istrate, M. A.; Busby, S. A.; Garcia-Ordóñez, R. D.; Burris, T. P.; Griffin, P. R. *Mol. Pharmacol.* **2010**, *77*, 228.
- See the [Supplementary data](#) for the experimental details associated with the co-crystal structure of compound **1** and the ROR α LBD. The coordinates and structure factors for the complex between ROR α and compound **1** have been deposited with the protein data bank and assigned the accession code 4NB6.
- Wurtz, J. M.; Bourguet, W.; Renaud, J. P.; Vivat, V.; Chambon, P.; Moras, D.; Gronemeyer, H. *Nat. Struct. Biol.* **1996**, *3*, 87.
- Jin, L.; Martynowski, D.; Zheng, S.; Wada, T.; Xie, W.; Li, Y. *Mol. Endocrinol.* **2010**, *24*, 923.
- Germain, P.; Staels, B.; Dacquet, C.; Spedding, M.; Laudet, V. *Pharmacol. Rev.* **2006**, *58*, 685.
- Zhang, W.; Zhang, J.; Fang, L.; Zhou, L.; Wang, S.; Xiang, Z.; Li, Y.; Wisely, B.; Zhang, G.; An, G.; Wang, Y.; Leung, S.; Zhong, Z. *Mol. Pharmacol.* **2012**, *82*, 583.
- Svensson, S.; Östberg, T.; Jacobsson, M.; Norström, C.; Stefansson, K.; Hallén, D.; Johansson, I. C.; Zachrisson, K.; Ogg, D.; Jenéber, L. *EMBO J.* **2003**, *22*, 4625.
- Hoerer, S.; Schmid, A.; Heckel, A.; Budzinski, R.-M.; Nar, H. J. *Mol. Biol.* **2003**, *334*, 853.
- The stabilization of His421 in LXR α and His435 in LXR β are important electrostatic interactions to hold helix 12 (a.k.a. AF2 helix) into a hydrophobic groove on the surface of the LBD near helices 3–5 and elicit agonist function of the respective receptors. For additional discussion of this histidine interaction, see Refs. 21,22 and Williams, S.; Bledsoe, R. K.; Collins, J. L.; Boggs, S.; Lambert, M. H.; Miller, A. B.; Moore, J.; McKee, D. D.; Moore, L.; Nichols, J.; Parks, D.; Watson, M.; Wisely, B.; Willson, T. M. *J. Biol. Chem.* **2003**, *278*, 27138.
- Xue, Y.; Chao, E.; Zuercher, W.; Willson, T. M.; Collins, J. L.; Redinbo, M. R. *Bioorg. Med. Chem.* **2007**, *15*, 2156.
- Salonen, L. M.; Ellermann, M.; Dieberich, F. *Angew. Chem., Int. Ed.* **2011**, *50*, 2.
- Both LXR receptor subtypes presented an aromatic amino acid residue (LXR α : Phe326 and LXR β : Phe340) in the same region as the Phe367 found in ROR α . The presence of Val355 in ROR α may also allow access to the π - π stacking interaction of **1** with Phe367; whereas, this region of the ligand binding pocket was partially occluded in the co-structures of **1** with LXR α and LXR β due to the presence of a larger isoleucine residue common to both LXR receptor subtypes (LXR α : Ile313 and LXR β : Ile327).
- See the [Supplementary data](#) for the biochemical and cellular assay details.
- The partition coefficient (log P) was calculated with internal software using the VolSurf approach. For additional details, see Cruciani, G.; Crivori, P.; Carrupt, P.-A.; Testa, B. J. *Mol. Struct.-Theochem.* **2000**, *503*, 17.
- Leeson, P. D.; Springthorpe, B. *Nat. Rev. Drug Discov.* **2007**, *6*, 881.
- Waring, M. J. *Expert Opin. Drug Discov.* **2010**, *5*, 235.
- Hansch, C.; Fujita, T. *J. Am. Chem. Soc.* **1964**, *86*, 1616.
- See Ref. 29 and Leach, A. R.; Hann, M. M.; Burrows, J. N.; Griffen, E. J. *Mol. Biosyst.* **2006**, *2*, 429.
- Hammitt, L. P. *J. Am. Chem. Soc.* **1937**, *59*, 96.
- A broader range of *para*-substituents for the aryl-sulfonamide was not considered due to excessively high clog P values (>5) for the final compounds combined with limited reagent availability.
- Anslyn, E. V.; Dougherty, D. A. *Advanced Concepts in Electronic Structure Theory. Modern Physical Organic Chemistry*, 1st ed.; University Science Books: USA, 2006. pp 850–853.
- Bissantz, C.; Kuhn, B.; Stahl, M. *J. Med. Chem.* **2010**, *53*, 5061.
- Brameld, K. A.; Kuhn, B.; Reuter, D. C.; Stahl, M. *J. Chem. Inf. Model.* **2008**, *48*, 1.
- Wang, Y.; Kumar, N.; Nuhant, P.; Cameron, M. D.; Istrate, M. A.; Roush, W. R.; Griffin, P. R.; Burris, T. P. *ACS Chem. Biol.* **2010**, *5*, 1029.
- Solt, L. A.; Kumar, N.; Nuhant, P.; Wang, Y.; Lauer, J. L.; Liu, J.; Istrate, M. A.; Kamenecka, T. M.; Roush, W. R.; Vidović, D.; Schürer, S. C.; Xu, J.; Wagoner, G.; Drew, P. D.; Griffin, P. R.; Burris, T. P. *Nature* **2011**, *472*, 491.
- Wilson, N. J.; Boniface, K.; Chan, J. R.; McKenzie, B. S.; Blumenschein, W. M.; Mattson, J. D.; Basham, B.; Smith, K.; Chen, T.; Morel, F.; Lecron, J.-C.; Kastelein, R. A.; Cua, D. J.; McClanahan, T. K.; Bowman, E. P.; De Waal Malefyt, R. *Nat. Immunol.* **2007**, *8*, 950.
- Li, L.; Liu, J.; Zhu, L.; Cutler, S.; Hasegawa, H.; Shan, B.; Medina, J. C. *Bioorg. Med. Chem. Lett.* **2006**, *16*, 1638.
- Supplemental ¹⁹F NMR experiments and/or ¹H-¹³C HMBC NMR experiments were routinely employed to insure the proper *N*-alkyl connectivity of the final compounds as drawn. For additional discussion, see Fauber, B. P.; Johnson, A. R.; René, O.; Bowerman, S.; Burton, B.; Colebrook, A.; Flynn, A.; Harrold, G.; Huhn, S.; Jones, G.; Lockey, P.; Norman, M.; Wong, H. *J. Labelled Comp. Radiopharm.* in press.
- Katritzky, A. R.; Pilarski, B.; Urogdi, L.; Katritzky, A. R.; Pilarski, B.; Urogdi, L. *Synthesis* **1989**, *12*, 949.
- Brameld, K. A.; Carter, D. S.; Chin, E.; Fidalgo, J.-V.; Li, J.; Schoenfeld, R. C.; Sjogren, E. B.; Talamas, F. X. US 2010/0021423.